Appl Phys A
DOI 10.1007/s00339-013-7901-2

Applied Physics A
Materials Science & Processing

Ultrafast laser ablation of metal films on flexible substrates

L. Gallais · E. Bergeret · B. Wang · M. Guerin · E. Bènevent

Received: 12 June 2013 / Accepted: 30 July 2013

Abstract For the development of organic electronics on flexible substrates, we study the potentialities of direct laser patterning of conductive films deposited on plastic foils. The materials under study are silver and platinum films (100-nm thick) deposited on Kapton® substrates. The experiments are done using a laser source operating at 1030 nm, 500 fs, under different irradiation conditions: single and multiple pulses at various frequencies. The laser ablation thresholds are measured and the ablation morphologies are analyzed with scanning electron microscopy. The results of these investigations show that photomechanical effects lead to delamination of the film and that depending of the irradiation conditions, incubation or heat accumulation effects can occur. The experimental results are compared to simulations based on the two-temperature model. Particularly we study the heat accumulation effects that can occur in the case of multiple pulses and that are detrimental for plastic substrates.

1 Introduction

Recently, the development of organic electronics materials has allowed to develop increasingly complex devices and in the same time to develop new associated process [1, 2]. The main advantage of organic devices on plastic substrates is their manufacturing cost. In order to maintain a fabrication cost as low as possible, new processes are studied. The organic materials are deposited owing to mass printing technology such as screen-printing or ink-jetting. Those processes can enable high-volume production and can be carried out in the open air. In order to pattern the deposited layers, the etching techniques, used in the silicon industry, can be replaced by the laser ablation. This etching process offers a precision similar to the one provided by the "classic" silicon chemical and physical etching at a lower cost. Indeed, the whole ablation process is made in open air and there is no need of solvent used. Moreover, the laser-ablated-target's heating remains minimal. A wide range of applications are possible in the electronics field. The main applications for organic electronic devices are the flexible solar cells, which are much cheaper than silicon-based ones, as well as organic sensors. Moreover, the field of the organic printed circuits is of interest too since it is now possible to develop organic diodes and transistors entirely made by cheap fabrication process and thus design organic circuits on plastic foils. Despite this recent progress, organic electronics still suffers from many problems, among them one of the most blocking is achieving rapid and non-resistive interconnections. Indeed, the lines carried by ink-jet printing have a poor conductivity due to the difficulty in carrying out ink metal particle. If recent efforts have improved the conductivity of these lines [3], it requires annealing processes that flexible substrates resent and still have a much lower conductivity than bulk materials.

Direct laser patterning on flexible substrates has been reported in the context of the fabrication of OLED devices, and the potentialities of the technique have been shown [4, 5]. In the present work, diodes, capacitors and pro-

L. Gallais (✉)
Institut Fresnel, UMR 7249, Aix Marseille Université, CNRS, Centrale Marseille, 13013 Marseille, France
e-mail: laurent.gallais@fresnel.fr

E. Bergeret · M. Guerin · E. Bènevent
IM2NP UMR 7334, Aix-Marseille Université, CNRS, 13397 Marseille Cedex 20, France

B. Wang
Department of Applied Physics, Nanjing University of Science & Technology, Nanjing 210094, P.R. China

Published online: 25 August 2013

grammable metallization cell memories are the subject of investigation. For these applications, the metallic layer must be removed precisely from the polymer substrate, without transferring heat to the substrate and to the surroundings of the laser irradiated area, thus leaving sharp edges and flat bottom. The advantages of femtosecond laser for precise material processing have been well established [6–8] and we have oriented our investigations in this area. Indeed, in the case of ablation with long laser pulses there is enough time for heat to penetrate the polymer substrate which has a low melting point temperature, and to melt the metal in the surrounding area [7]. However, an efficient use of femtosecond laser processing requires a detailed knowledge of the physical processes that govern the ablation mechanism. Systematic studies of laser–matter interaction in our particular samples is therefore necessary to establish scaling laws and identify the best conditions to operate. In addition, the metal films under study (silver and platinum) can have very different properties from their bulk counterparts. The first part of the paper is dedicated to the description and measurements of the samples: the fabrication conditions are described, and electrical (for functional operation) as well as optical (for laser processing operation) characterizations are conducted. For the best results, the low-fluence regime (closed to the ablation threshold) is the most interesting for material processing, since in this case the energy deposited into the metal and the heat-affected zones is being minimized [7]. A study of the ablation threshold as a function of the laser irradiation parameters (single or multiple pulses at different repetition rates) is therefore conducted.

In the first part of the paper the experiments are described and the measurements methods are detailed. The ablation threshold and morphologies are then reported, for 1030 nm/500 fs irradiation with different pulse sequences. In the last part a discussion on the physical processes involved in our operating conditions is conducted, with simulations based on thermal models.

2 Samples

The materials under study have been targeted to be used for creating flexible capacitors, filters, inductors and active interconnection devices. The common flexible substrates used for electronic applications are polyethylene terephthalate (PET), polyethylene naphthalate (PEN) and Kapton®. For this study, a 50-µm-thick Dupont Kapton sheet is chosen as a flexible substrate, mainly because of its higher resistance to high temperatures. Indeed, the maximum process temperatures of the PEN and PET are below 150 °C while a Kapton sheet remains intact for temperatures up to 400 °C. And some inks (in particular conductive inks) need a thermal treatment approaching 150 °C.

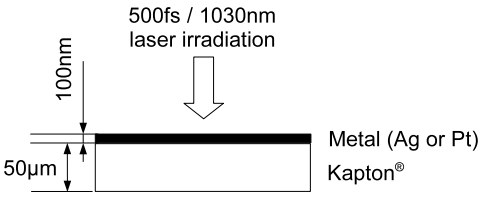

Fig. 1 Samples description and laser irradiation conditions

2.1 Fabrication

The metallic layers consist of a 100 nm platinum or silver bottom layer deposited under vacuum by an RF sputtering technique without any thermal post-process. The silver layer can also be deposited by inkjet methods or spin coating and form a conductive layer after a 300 °C annealing.

The schematic of the samples and irradiation condition is given in Fig. 1.

2.2 Characterization and properties

The thin metal films can have electronic and optical properties very different from bulk materials, because of both their low thickness and their manufacturing process. In addition, it is difficult to estimate these properties based on similar works since they can be very dependent on the deposition process, substrate material and starting source. We have therefore conducted a characterization of the films to evaluate their potentialities for applications (electronic properties) and for the ablation process (optical properties).

Electronic properties Several lines of different dimensions were performed on silver by laser ablation. These lines have been measured to determine the conductivity of the deposited platinum and silver layer. Line width is from 14 to 140 µm. The measured conductivity is presented in Figs. 2 and 3. The conductivity of the laser patterned line is compared to bulk conductivity and thin-film conductivity calculated owing to Fuchs–Sondheimer model [9, 10]. Measured conductivity is in good agreement with the predicted one for 100 nm thickness.

An important point is that to achieve these lines no photolithography mask was needed, which makes the method of realization as flexible as the inkjet, but the conductivity is more important than recent study made by inkjet (Table 1). This is one of the advantages of the use of laser ablation on flexible substrate: the design of structures can be done on materials with good electrical properties without annealing. Moreover, laser can do the pattern in one pass whereas the inkjet needs many passes to have sufficient thickness on the line.

The reflectance of the samples was measured under quasi-normal incidence from 260 nm (4.75 eV) to 1500 nm (0.83 eV) with 5-nm resolution, using a Perkin Elmer

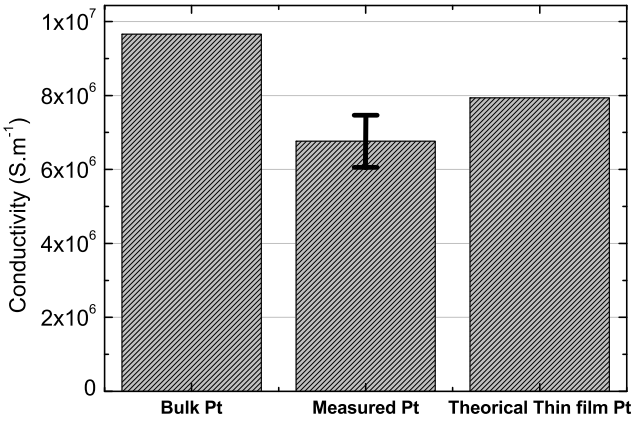

Fig. 2 Measured laser ablated line conductivity on a 100 nm Pt

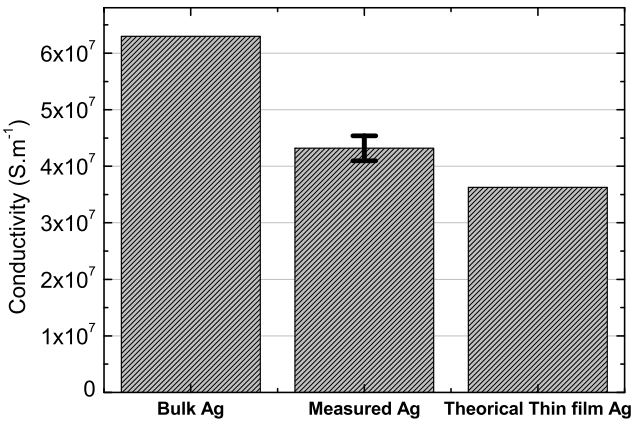

Fig. 3 Measured laser ablated line conductivity on a 100 nm Ag

Table 1 Conductivity of the samples and comparison to several references

Material	Silver ink [3]	Silver ink [11]	Silver this work
Line design method	Inkjet	Inkjet	Laser ablation
Conductivity (MS m^{-1})	5	32.3	43.2
Cured	150 °C	500 °C	–

lambda 1050 spectrophotometer. The results of the measurements are given in Figs. 4 and 5. For the sake of comparison, a plot for the case of bulk materials (extracted from Ref. [12]) is also given.

Optical properties In the case of platinum, the film reflection is very closed to the bulk value in the whole measurement range, which means that the optical properties of the film can be considered the same as the bulk ones. In the case of silver there is a significant difference between film and bulk reflection, particularly at the wavelength of the study (1030 nm): the measured reflection is 92.6 % for the film

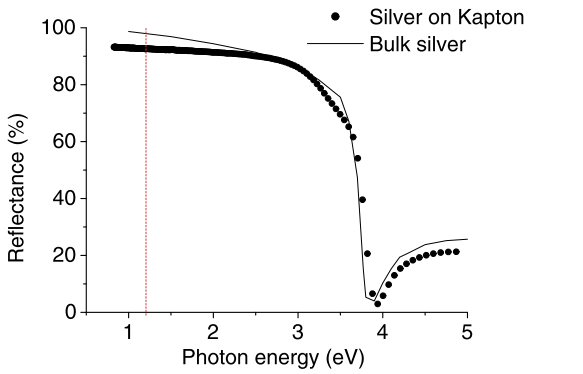

Fig. 4 Measured reflection on a 100-nm silver film on a Kapton surface and comparison with the bulk material. The *red line* indicates the laser irradiation photon energy used in the ablation experiments

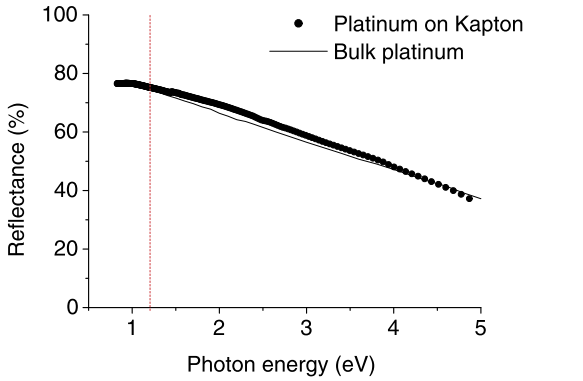

Fig. 5 Measured reflection on a 100-nm platinum film on a Kapton surface and comparison with the bulk material

compared to 98 % for the bulk material. We have therefore measured a film sample deposited in the same conditions but on a glass substrate. This sample has the same reflectivity (98 %) as the bulk material. We then assume that the silver film has the same refractive index and hence absorption as the bulk material and that the difference of reflectivity is related to a substrate effect. An increase of scattering losses due to the substrate roughness is one possibility.

3 Experiments

3.1 Experimental setup

The facility used to study the ablation threshold of the samples is described in detail in Ref. [13]. The laser source is a commercial femtosecond-diode-pumped ytterbium amplified laser (Amplitudes Systemes S-Pulse HP) with a spatially Gaussian beam profile. The operating wavelength is 1030 nm with 5-nm spectral bandwidth. The pulse duration was set to 500 fs (an auto-correlation trace is given in Fig. 6). The laser was operated with a repetition rate of 10, 100 or 1000 Hz in this study. A mechanical shutter has been used to deliver single shots or a burst of pulses on the sample. The

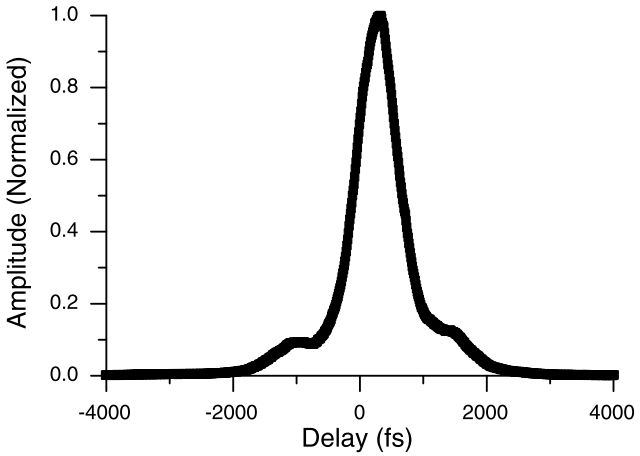

Fig. 6 Autocorrelation trace of the femtosecond laser acquired with an Avesta ASF system

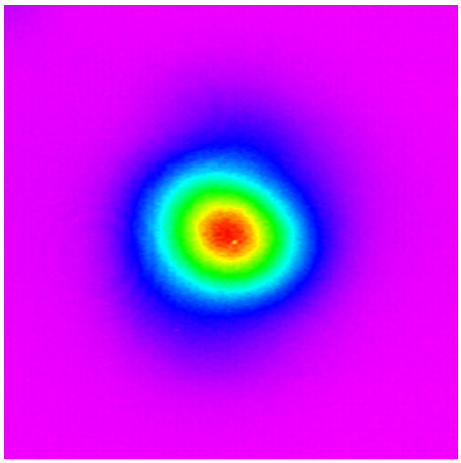

Fig. 7 Image of the laser beam in the sample plane

pulse energy can be continuously modified using a combination of a half-wave plate and a thin-film polarizer. A beamsplitter fixed after the polarizer directs a small portion of the pulse to a pyroelectric detector for energy measurement after each shot. Calibration is realized before test with another pyroelectric detector located after the focusing lens. At 10 Hz the single-pulse energy was measured with the pyroelectric detector. At higher repetition rates (100 Hz and 1 kHz), a power meter was used for determination of the mean output power. The linearly polarized laser beam is focused at normal incidence onto the front face of the coated sample by a plano-convex lens (focal length $f = 150$ mm). The spatial beam profile was measured at the location of the sample plane with a CCD camera and a magnification system. The beam diameter is 55 µm at 1/e (Fig. 7).

3.2 Measurement procedure

The objective of the tests is to determine as accurately as possible the ablation thresholds in conditions that are representative of possible laser processing parameters for practical applications. Then relative low frequencies were studied (up to 1 kHz) to avoid heat accumulation effect and the case of multiple pulses (from 1 to 1000) was tested in order to investigate the accumulation effect that can occur in the case of direct laser patterning on metals. The determination of the ablation threshold fluences (F_{th}) has been done with two methods. Firstly, by plotting the squared diameter (D^2) of the laser-ablated area as a function of the incident maximum fluence (F) on the sample, according to the procedure described in Ref. [14]. A fit of the data with the following relation is done:

$$D^2 = 2\omega^2 \ln\left(\frac{F}{F_{\text{th}}}\right) \tag{1}$$

with ω the beam waist radius, assuming that the beam is spatially Gaussian (which was the case in these experiments). The diameter measurements are done with an Axiotech Zeiss optical microscope.

However, for particular cases corresponding to long irradiation times on each site (for instance, 1000 shots at 10 Hz), the heat has time to diffuse out of the irradiated area and the previous ablation threshold determination, based on the fact that a modification occurs only under the surface of the spot where the fluence is greater than F_{th}, is not applicable anymore. In this case the relation (1) is not suitable. Therefore the threshold has also been measured with a second method: it is defined as the highest threshold where no modification of the surface is observed after irradiation (under a Nomarski microscopy). A comparison of both threshold estimations will be done in the following.

4 Results

4.1 Ablation thresholds

Silver Figure 8 shows the squared diameter of the damaged areas as a function of the logarithm of the pulse fluence, for different pulse numbers, with a repetition rate of 10 Hz. By extrapolations of the fits one can obtain the ablation threshold from the formula (1).

It appears that for 100 and 1000 pulses, the linear relationship between the squared diameter of the damaged area and the logarithm of the fluence is no longer available, which can be linked to thermal effects as exposed previously, and a different threshold determination procedure is needed in this case. The ablation thresholds are reported in Fig. 9 for the different irradiation conditions that were tested, and for the two threshold determination procedures.

In the case of 1 or 10 shots, the two evaluated thresholds are in good accordance. However, for 100 and 1000 pulses, as said before, there is a clear difference of thresholds obtained by the two determination methods at the different frequencies of test. This is particularly true at 1000 Hz. The

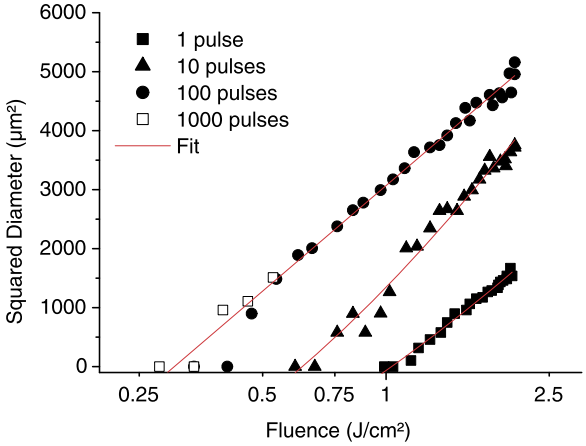

Fig. 8 Squared diameter of the laser-ablated areas on the 100-nm silver layer on Kapton, as a function of the number of pulses per spot. For these measurements, the repetition rate is 10 Hz

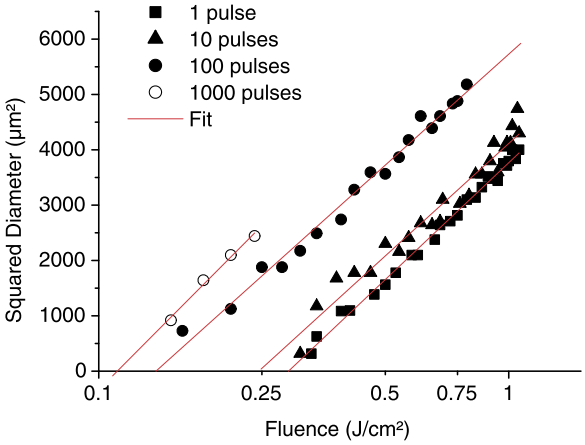

Fig. 10 Squared diameter of the laser-ablated areas of the 100-nm platinum layer on Kapton, as a function of the number of pulses per spot. The repetition rate is 10 Hz

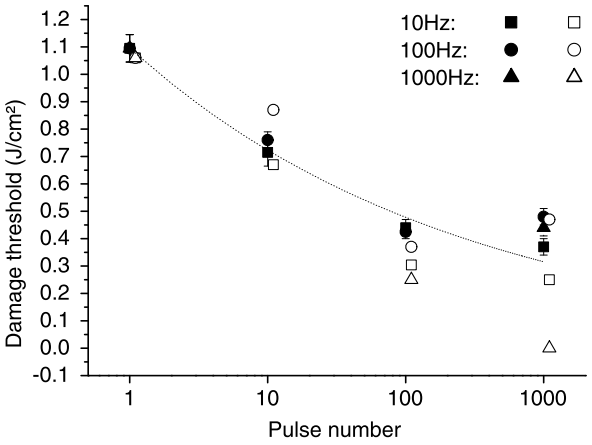

Fig. 9 Damage thresholds of a 100-nm silver layer on a Kapton sample as a function of the number and frequency of pulses. *Filled symbols*: threshold determination based on visual criteria (highest fluence at which no modification is observed). *Empty symbols*: threshold determination based on the assumed relationship $D^2 = 2\omega^2 \ln(\frac{F}{F_{\text{th}}})$. The *dotted line* is a plot of the incubation equation described in the text with $\xi = 0.82$

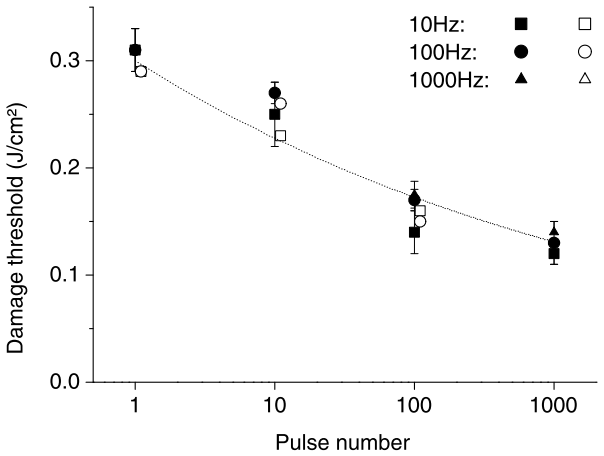

Fig. 11 Damage thresholds of a 100-nm platinum layer on a Kapton sample as a function of the number and frequency of pulses. *Filed symbols*: threshold determination based on visual criteria (the highest fluence at which no modification is observed). *Empty symbols*: threshold determination based on the assumed relationship $D^2 = 2\omega^2 \ln(\frac{F}{F_{\text{th}}})$. The *dotted line* is a plot of the incubation equation described in the text with $\xi = 0.88$

method based on the logarithmic dependence of the ablated surface to the applied fluence is clearly non-applicable because of thermal issues. These thermal effects will be seen in the SEM images that are given in Sect. 4.2. Looking at the results of the thresholds determined by visual criteria, we observe a decrease of the threshold with the number of pulses, characteristic of an incubation behavior that is known to occur in many materials. Without analyzing yet the causes of this behavior we can use the empirical description proposed in [15]:

$$F_{\text{th}}(N) = F_{\text{th}}(1)N^{\xi-1} \tag{2}$$

with $F_{\text{th}}(N)$ the threshold fluence for applying N pulses to the same area and ξ the exponent that characterizes the degree of incubation. An incubation coefficient of $\xi = 0.82$ was determined for the silver samples (dotted line in Fig. 9).

Platinum The results for the case of platinum films are given in Figs. 10 and 11.

Contrary to the case of silver, we observe for this material a coherence between the results given by the two detection methods. This indicates that the ablation threshold is directly linked to the local intrinsic absorption properties of the film, and less affected by transverse heat diffusion in the film. This will be evidenced by the morphologies in the next section. The ablation threshold is decreasing with the pulse number and the incubation coefficient is $\xi = 0.88$.

Table 2 Comparison of results to published data

	$F_{th}(1)$	ξ	Conditions	Ref.
Ag film (100-nm on Kapton)	1.1 ± 0.05 J/cm^2	0.82	1030 nm, 500 fs 10 Hz–1 kHz	Present work
Ag (bulk)	1.5 ± 0.4 J/cm^2	0.87 ± 0.05	800 nm, 100 fs 10 Hz–1 kHz	[16]
Ag film (200-nm on BK7)	0.8 J/cm^2 (film modification) 3 J/cm^2 (film ablation)		800 nm, 120 fs 1 kHz	[17]
Ag film (on BK7)	0.69 ± 0.07 J/cm^2		1054 nm, 400 fs	[18]
Pt films (100-nm on Kapton)	0.31 ± 0.02 J/cm^2	0.88	1030 nm, 500 fs 10 Hz–1 kHz	Present work

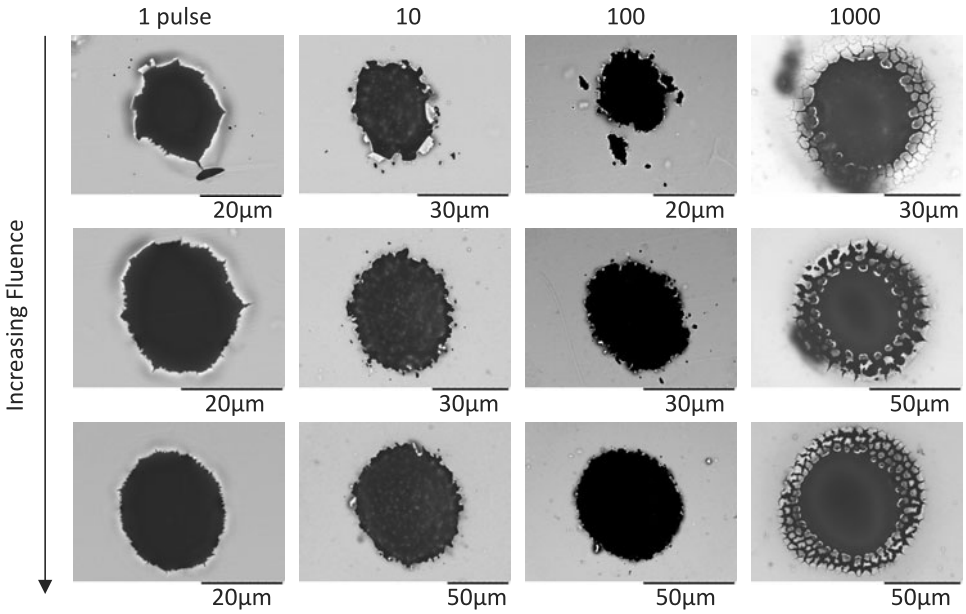

Fig. 12 SEM images of the laser irradiated sites on silver samples with 1, 10 (10 Hz), 100 (10 Hz) and 1000 (1 kHz) pulses. The *scales* are not the same on all the images

Comparison to published data We have tried to compare our results (ablation thresholds and incubation coefficient) to published data for the two metals under investigation. However, very few data are available for femto/picosecond irradiation of silver and platinum, particularly for the case of platinum. We have summarized our results and compared them to other available data in Table 2.

For the case of platinum, our work seems to be the first precise determination of ablation thresholds. For the case of silver, our results are in very good agreement with the work of Byskov-Nielsen et al. [16] where the experiments were done in approximately similar conditions (wavelength, spot size, pulse duration, repetition rate), except that they have studied bulk polished silver samples. In the other work (Dai et al. [17]), where silver films were studied, the definition of damage was not clear since they were interested in nanostructuring of the films. However, the range of value is in accordance with our results.

4.2 Ablation morphologies

The laser irradiated areas were observed with Scanning Electron Microscopy (Hitachi TM-1000) and Nomarski microscopy (Zeiss Axiotech). The SEM images are reported in Figs. 12 and 13 for silver and platinum, respectively. We have not observed significant differences in the damage morphologies when the repetition rate is changed (excepted at 1 kHz for silver), so only the results at one frequency are given.

In the case of platinum we observe, whatever the irradiation conditions, an ablation mechanism that is related to mechanical effects: the layer is delaminated from the substrate, without any evidence of the melting of the metal. Near the crater edges, some parts of the film have been lifted off and are still being attached to the film, which support the athermal character of the ablation. This is also the case for the silver samples, but only with a low pulse number as it can be seen in the SEM images. The example in Fig. 14 illus-

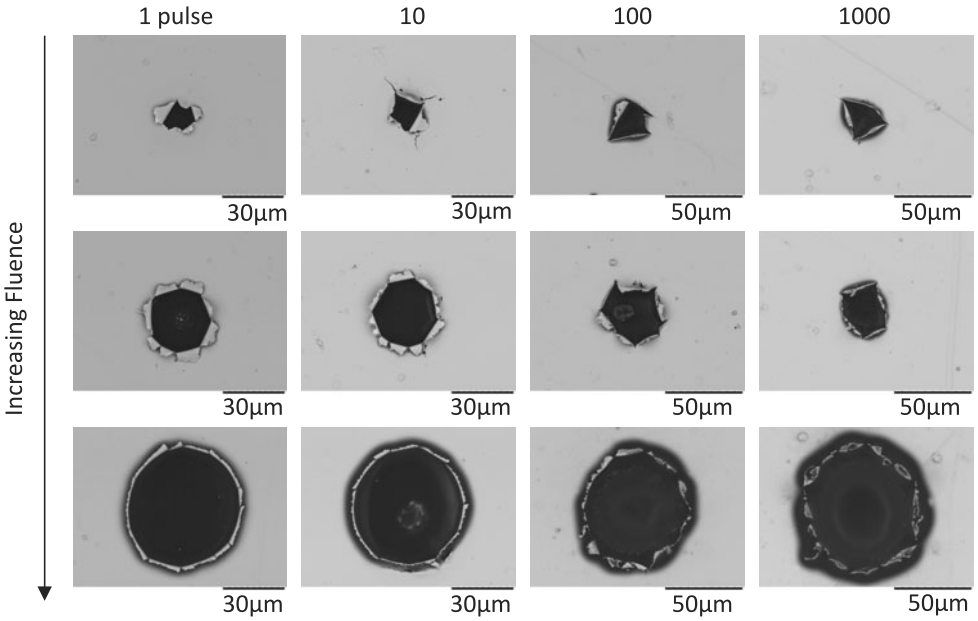

Fig. 13 SEM images of the laser irradiated sites on platinum samples with 1, 10 (10 Hz), 100 (10 Hz) and 1000 (1 kHz) pulses. The *scales* are not the same on all the images

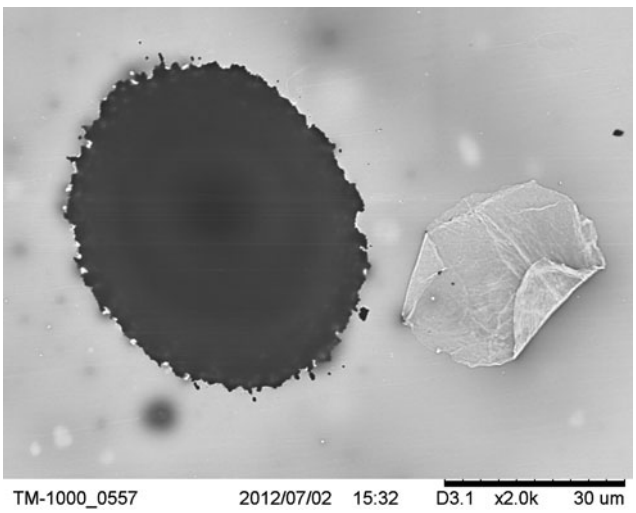

Fig. 14 SEM image on the silver film, irradiated at 0.88 J/cm^2 with 100 pulses at 10 Hz. On the *right* of the image the part of the film that has been removed from the substrate can been seen

trates clearly this mechanism where the film has been totally removed without being heat-affected.

From these observations, the ablation mechanism appears to be photo-induced laser spallation. The stresses and shock-waves generated in the film by laser irradiation lead to the disruption of the film/substrate interface, and ejection of the film. This mechanism is of interest for practical application since the layer can be removed without strong thermal effects such as melting and evaporation that could damage the substrate. However, the drawback is that the edges of the ablated sites are not sharp. We will analyze further the involved mechanisms in the next section.

5 Analysis

When irradiated by the laser, the free electrons in the metal film will strongly absorb the laser energy. In the case of sub-picosecond pulses, the timescale at which absorption occurs is such that the electron subsystem has not enough time to transfer its energy to lattice during the pulse. Energy transfer via electron–phonon interactions occurring after the laser pulse will induce heating of the lattice and later in time subsequent physical degradation through different possible mechanisms [19]. In order to remove the metal film from the substrate, sufficient energy must be provided by the laser beam to remove the film. With a first-order approach we can estimate the irradiation fluence needed to melt the film:

$$F_{\text{melt}} = A * C\rho d(T_{\text{melt}} - T_0) + A * \rho d H_{\text{melt}} \tag{3}$$

with F_{melt} the fluence needed for melting (J), C the heat capacity ($\text{J} \times \text{kg}^{-1} \times \text{K}^{-1}$), ρ the density ($\text{kg} \times \text{m}^{-3}$), T_{melt} the melting temperature, T_0 the ambient temperature, d the film thickness (m), H_{melt} the enthalpy of fusion/vaporization ($\text{J} \times \text{kg}^{-1}$) and A the absorption coefficient. From these simple calculations, the energy needed to melt a 100-nm film of silver is 1.8 J/cm^2 and it is 0.3 J/cm^2 for the case of platinum, considering the material parameters given in Table 3. Of course these estimated values are expected to be different from experiments since all the parameters are assumed to be constant. Particularly, the absorption will increase during the pulse for high electronic temperatures, as predicted by Drude and derivatives models [20]. This will induce a better coupling of the energy in the metal and a decrease of the energy needed for fusion/vaporization. However the values are close to the experimental results: 1.1 J/cm^2 for silver and 0.3 J/cm^2 for platinum. To have a better description of the

Table 3 Summary of the different physical properties of silver and platinum, extracted from Ref. [12]

Metal	Optical index	Absorption coefficient	Density ($kg \times m^{-3}$)	Heat capacity ($J \times kg^{-1} \times K^{-1}$)	Melting temperature (°C)	Fusion enthalpy ($J \times kg^{-1}$)
Silver	0.28+i*7.5	0.02	$1.05e^4$	235	962	$1.05e^5$
Platinum	3.55+i*5.92	0.25	$2.15e^4$	133	1768	$1.14e^5$

Table 4 Material parameters used for TTM calculations. The values for the electron heat capacity, C_e, and electron-coupling term, μ, are based on fits of the theoretical results published in Ref. [22]

Metal	μ ($W m^{-3} K^{-1}$)	C_e ($J m^{-3} K^{-1}$)
Silver	2.8×10^{17} for $T_e \leq 4000$ K $-2.96 \times 10^{18}/(1+(T_e/11800)^{3.23}) + 3.14 \times 10^{18}$	$63.3 * T_e$ for $T_e \leq 4000$ K $-3.9 \times 10^6/(1+(T_e/11300)^{3.03}) + 4 \times 10^6$
Platinum	$2.3e17 + 8.8e17 * \exp(-T_e/3100)$	$145 * T_e + 150000$

dynamics of the energy deposition, we have used a classical approach with the two-temperature model [21].

5.1 Two-temperature model

The two-temperature model describes the energy transfer and the temperatures of electrons (T_e) and lattice (T_l) in a solid submitted to a laser irradiation at the femtosecond timescale. These temperatures can be calculated by solving the coupled heat conduction equations of electrons and lattice:

$$C_e \frac{\partial T_e}{\partial t} = \nabla(K_e \nabla T_e)) - \mu(T_e - T_l) + S(z,t) \quad (4)$$

$$C_l \frac{\partial T_l}{\partial t} = \nabla(K_l \nabla T_l)) + \mu(T_e - T_l) \quad (5)$$

with C_e and C_l the specific heat capacities ($J m^{-3} K^{-1}$) of the electrons and the lattice, respectively, K_e and K_l the corresponding thermal conductivity coefficients ($W m^{-1} K^{-1}$), the parameter $\mu = C_e/\tau$ characterizing the rate of energy exchange ($W m^{-3} K^{-1}$) between the electron and lattice subsystems (τ is the characteristic exchange time for the electron subsystem), and $S(z,t)$ the heat source term induced by the laser irradiation ($W m^{-3}$). The electron heat capacity depends on the temperature and a linear dependence is often used in TTM calculations, as a temperature-independent electron coupling factor [21]. However, theoretical studies based on electronic structure calculations of the electron densities of states predict large variations from these used approximations [22]. For a better computational analysis, we used for C_e and μ the temperature dependencies calculated in Ref. [22]. The thermal conductivity depends on both the electron and lattice temperatures and can be expressed as $K_e = \frac{1}{3} v_F^2 \tau C_e$, where v_F is the electron Fermi velocity and τ is the electron relaxation time that takes into account both electron–phonon and electron–electron contributions. For its description, we used an empirical model [23]: $1/\tau = AT_e^2 + BT_i$ with A and B assumed to be constant. The different parameters used in the simulations and the corresponding references are given in Table 4.

Given that the thickness of the film (100 nm) is larger than the optical absorption depth in silver and platinum, there is no source term in the substrate. Then the source in the film can be described by a Beer–Lambert law:

$$S(z,t) = \alpha A I(t) e^{-\alpha z} \quad (6)$$

with A the absorption coefficient, $I(t)$ the laser intensity as a function of time ($W m^{-2}$) and α the absorption coefficient (m^{-1}). In the following simulations we will consider a pulse of constant intensity I_0 during the pulse width t_0. A plane wave is assumed as the irradiation condition, then the source term and hence the temperature are dependent on the spatial coordinate z only.

The results of the simulations for the case of a silver film on Kapton corresponding to the conditions of the experiments are given in Fig. 15.

In the case of silver, the temperature of electron and lattice needs around few picoseconds to come to a balance. When the laser pulse duration is 500 fs, at a fluence close to the observed ablation threshold (1.1 J/cm^2) the electron temperature reaches around 10,000 K before the heat transfer to the lattice. At this fluence, the maximum lattice temperature reached in the film is around 3000 K, which is largely higher than the melting point of silver. However, this temperature is reached only on a 10-nm depth, and in few tens of picosecond the whole film is thermalized to the same temperature. This temperature is found to be around 2000 K for 1 J/cm^2, which is higher than the melting point of silver (we have found that the films were not melted) but in the same order of value (a lot of approximations are done in the model). The theoretical fluence to be below the melting point of the film is 0.6 J/cm^2 with our calculation parameters. The heating process of the film is then in the order of 20 ps, and for cooling down it takes less than one nanosecond. During this time the substrate is heat-affected only in less than 20 nanometers

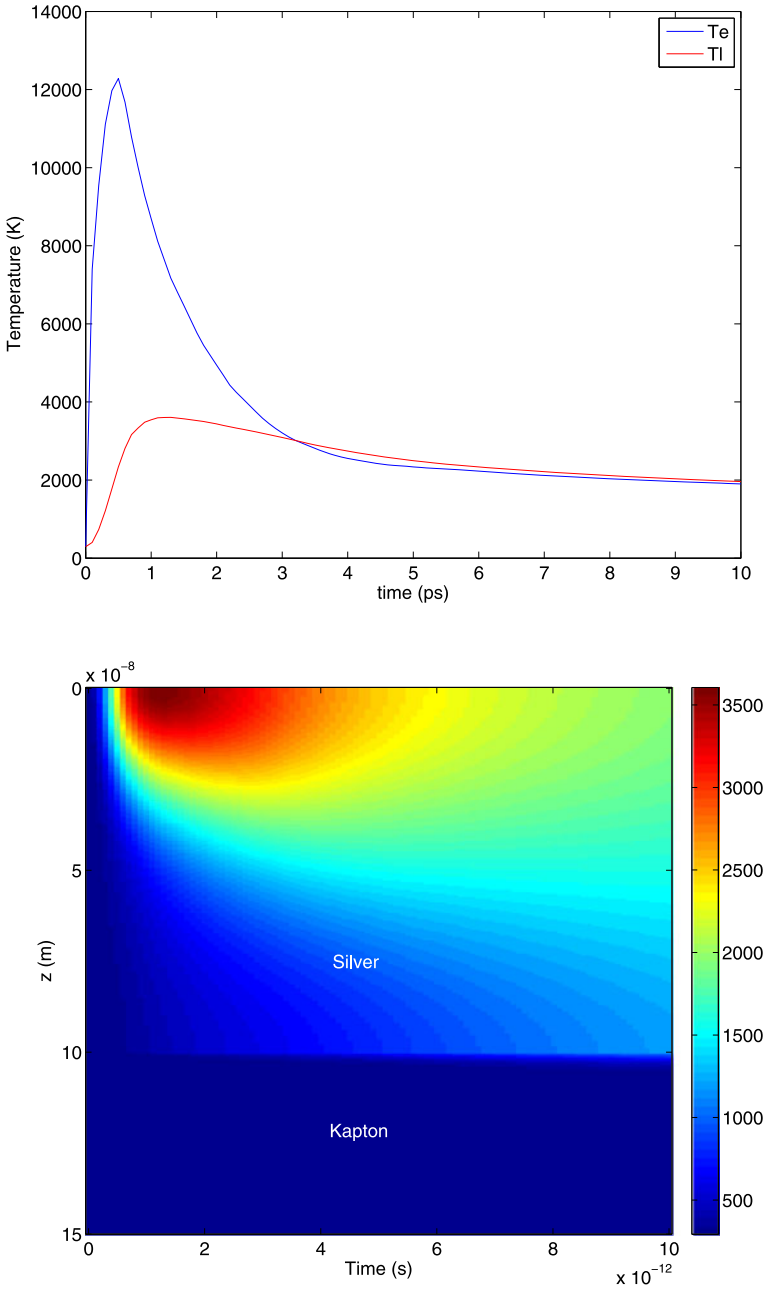

Fig. 15 Two-temperature model calculations applied to the case of a silver film (100 nm) on Kapton. A laser irradiation of 1 J/cm^2 is applied during 500 fs (starting at $t = 0$ s). The *upper image* is the evolution of the electronic (T_e) and lattice (T_l) temperatures at the surface of the film ($z = 0$). The *bottom image* is a representation of the evolution of the lattice temperature as a function of z ($z < 0$ in the air, $0 < z < 100$ nm in the film and $z > 100$ nm in the Kapton substrate

in depth and the temperature is higher than the melting point of Kapton in less than 10 nm. Then in the case of a single-shot irradiation, the thermal effects in the substrate should be limited.

The case of platinum is reported in Fig. 16. The calculation is done at 0.3 J/cm^2, which corresponds to the observed ablation threshold.

For the platinum the maximum electronic temperature reached under our calculation parameters and at 0.3 J/cm^2 is around 30,000 K, and the temperature decreases very quickly after the pulse down to 10,000 K. The lattice temperature reaches 8000 K at the maximum value on the surface and after few tens of picoseconds the whole film is thermalized at 3000 K. As for the case of silver, the temperature reached in platinum is higher than the melting point in almost the same ratio:

- silver has a melting point of 1240 K and we found a maximum temperature of 3000 K and a temperature of 2000 K after heat distribution in the film.
- platinum has a melting point of 2045 K and we found a maximum temperature of 8000 K and a temperature of 3000 K after heat distribution in the film.

Calculations based on the 2T model show that the melting temperature should be reached, whereas no evidence of

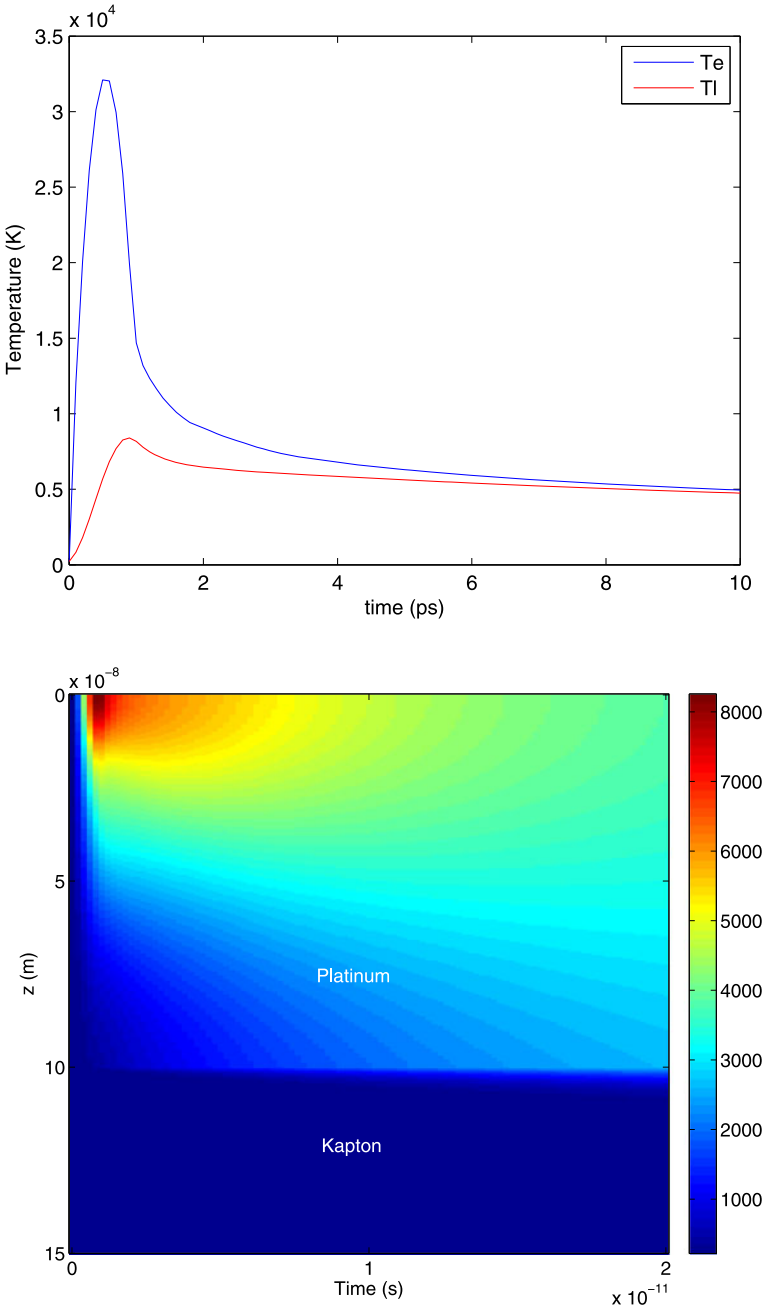

Fig. 16 Two-temperature model calculations applied to the case of a platinum film (100 nm) on Kapton. Same calculations as the ones shown in Fig. 15 but for the case of an irradiation of 0.3 J/cm^2

melting has been observed on the samples. Then the calculated temperature appear to be overestimated by the model with the material properties which have been used. As mentioned previously, there are few experimental data published on the metals under investigation and the pertinence of the used theoretical values of parameters for silver and platinum can be questioned.

5.2 Material ejection mechanism

The experimental results have demonstrated that in the case of a single-pulse irradiation, the layer is removed from the substrate without being heat-affected (see Fig. 14 for instance). Photo-induced mechanical effects are then responsible for the removal of the film. For a complete description of these effects a molecular dynamic modeling would be required, such as in Ref. [24] or [25], which is well above the objectives of this work. We will then base our analysis on qualitative discussions for a basic understanding of the processes.

According to the previous section, in the cases of silver and platinum the film is homogeneously heated at high temperature in less than 20 ps. Considering the thickness of 100 nm of the film, the thermalization takes place at a speed

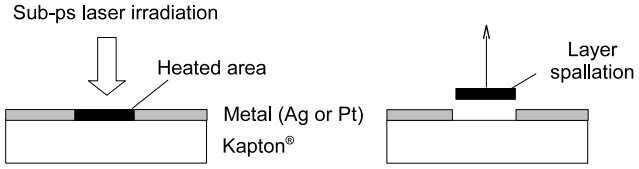

Fig. 17 Schematic of the shock-assisted ablation mechanism occurring for the case of silver and platinum films on a Kapton substrate

of 2×10^4 m/s, which is a factor of five above the acoustic wave speed propagation in both materials (Table 5). Such conditions where the laser pulse heats the film isochorically faster than the thermal expansion can occur, are typical for shock-wave assisted ablation [26]. The corresponding mechanism is summarized in Fig. 17. After laser heating, the irradiated film area undergoes rapid thermal expansion. Considering the calculated lattice temperature in the previous section and the thermal coefficient expansion coefficient given in Table 5 one can find a relative expansion (δ) of 3.2×10^{-2} for silver and 2.3×10^{-2} for platinum. The substrate is not heat-affected during the first stage of the process, and resulting from the expansion of the film a high compressive stress builds up at the interface. The compressive stress that is generated by instantaneous compression of the material can be estimated as $\sigma_c^{\text{inst}} = Y\delta$ where Y is the elastic modulus of the layer [27]. Using the values of Table 5, we evaluate the compressive stress as 2.7 GN/m^2 for silver and 3.9 GN/m^2 for platinum. The present estimation indicates that the values reached for both materials are in the same order of magnitude. Such high stresses can overcome the interface strength (unknown in our case but there is no strong adherence of the film to the substrate) and are largely beyond the yield strength of silver and platinum (Table 5).

5.3 Incubation and heat accumulation effects

Single or multiple pulses can be used to remove the metal from the film. In the case of repetitive pulses, we have described in Sect. 4.1 the incubation behavior that has been observed, with the use of an incubation coefficient (ξ). This coefficient was found to be 0.82 for silver and 0.88 for platinum. These values that correspond to the case of a thin film, can be compared to other data obtained in the case of bulk metals: Byskov-Nielsen et al. [16] have found a value of 0.87 for silver at 800 nm/100 fs (and 0.85 for copper and 0.84 for tungsten). No other data were found for silver or platinum, but in the case of copper, values of 0.76 (800 nm/120 fs) [28], 0.87 (800 nm/150 fs) [29] and 0.85 (800 nm/100 fs) [16] were obtained, for tungsten 0.84 (800 nm/100 fs) was found [16], 0.88 (800 nm/150 fs) [29] for niobium, 0.83 (800 nm/150 fs) [29] for titanium and 0.86 (800 nm/150 fs) [29] for stainless steel. It appears that a similar behavior is observed for different metals with different physical properties and it is also observed in our case of thin metal films. The involved mechanisms are, however, still not clear and different explanations have been proposed such as the accumulation of stress and plastic deformation [30], increase of absorption and energy coupling due to roughening of the surface or the occurrence of ripples after multiple irradiations [29]. These physical effects are not frequency-dependent for our operating conditions (lower than 1 kHz) but as it has been observed with our experimental results, other effects due to thermal accumulation can occur and modify the incubation law.

With the use of repetitive pulses for laser processing, heat accumulation effects can occur depending on the number of pulses and the repetition rate, which can damage the substrate and/or leave heat-affected edges around the removed metal film. This effect has been observed for the case of silver submitted to 1000 pulses (Fig. 12) but not for the case of platinum. In order to evaluate the thermal effects induced by multiple pulses, the previously described temperature model can easily be applied to the calculation of the temperature rise induced by repetitive pulses. The response of the material to a train of pulses can be written as

$$T(z,t) = \sum_{n=0}^{int(t\times F)} T_{1\text{pulse}}(z - nT) \tag{7}$$

with $T_{1\text{pulse}}$ the response to a single pulse, F the repetition rate, and $int(t \times F)$ the number of pulses that have irradiated the material between the time 0 and t. In order to determine the influence of the thermal accumulation effects in the two metals, we have calculated the fluence needed to reach the melting point of the metal (as an arbitrary criterion to compare the results) as a function of the pulse number. We have conducted this calculation at 1000 Hz, where the effect has been experimentally observed. The results of these calculations are given in Fig. 18.

In the case of silver, there is a decrease of a factor of approximately 3 between one pulse and 1000 pulses. This can explain the deviation that we have observed from the incubation behaviors seen at lower frequencies (Fig. 9) and

Table 5 Thermo-mechanical properties of silver and platinum, extracted or calculated (speed of sound) from [12]

Metal	Young's modulus (GN/m^2)	Coeff. linear expansion (K^{-1})	Compression sound wave (m/s)	Yield strength (MN/m^2)
Silver	82.7	18.9×10^{-6}	3700	130
Platinum	170	8.8×10^{-6}	4000	150

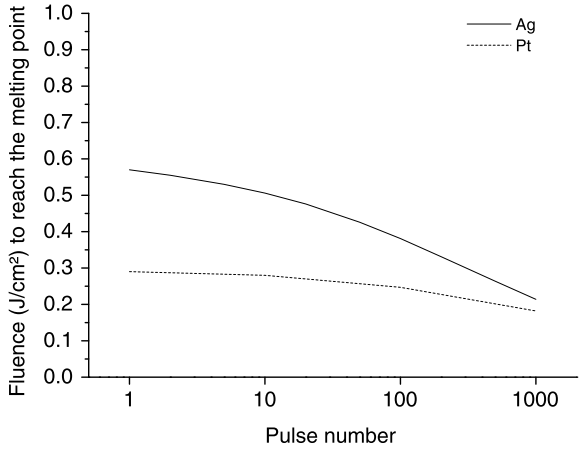

Fig. 18 Theoretical fluence needed to reach the melting point of the metal as a function of the pulse number. The calculation is done using the material parameters given previously for silver, platinum and Kapton, with a pulse repetition rate of 1000 Hz

the morphologies (Fig. 12). Since the silver film is very sensitive to thermal accumulation at that frequency, low pulse numbers must be used to avoid thermal effects in practical operating conditions or lower frequencies at the detriment of the processing speed. For comparison, at 100 Hz the decrease is of the order of 30 % and negligible at 10 Hz. In the case of platinum, however, if a decrease of 30 % can be observed, it is of the same order as the incubation effects and it does not seem to play a role in the damage process (no evidence of thermal effects in the morphologies and no deviation from the behaviors at other frequencies).

6 Conclusions

We have reported on the laser ablation threshold of silver and platinum films deposited on a polymer substrate and irradiated in the sub-picosecond regime. Precise thresholds and incubation coefficient were obtained as the conductivity and optical properties. These data are of practical interest for the laser processing of Ag and Pt films for organic electronics applications. In addition, the observed damage morphologies have revealed that the layer is ejected, possibly by a stress-assisted process as it has been discussed based on theoretical estimations, without any evidence of melting if the frequency is kept low. Such conditions are particularly interesting to the design of electronic devices on flexible substrates.

Acknowledgements We gratefully acknowledge the Mission des Ressources et Compétences Technologiques from the Centre National de la Recherche Scientifique for their financial support.

We thank F. Lemarchand (Institut Fresnel) for the spectrophotometric measurements.

References

1. A.C. Hubler, G.C. Schmidt, H. Kempa, K. Reuter, M. Hambsch, M. Bellmann, Org. Electron. **12**, 419 (2011)
2. N.A. Azarova, J.W. Owen, C.A. McLellan, M.A. Grimminger, E.K. Chapman, J.E. Anthony, O.D. Jurshescu, Org. Electron. **11**, 1960 (2010)
3. X. Nie, H. Wang, J. Zou, Appl. Surf. Sci. **261**, 554 (2012)
4. D. Karnakis, A. Kearsley, M. Knowles, J. Laser Micro Nanoeng. **4**, 218 (2009)
5. R. Mandamparambil, H. Fledderus, G. Van Steenberge, A. Dietzel, Opt. Express **18**, 7575 (2010)
6. S. Preuss, A. Demchuk, M. Stuke, Appl. Phys. A **61**, 33 (1995)
7. B.N. Chichkov, C. Momma, S. Nolte, F. Von Alvensleben, A. Tunnermann, Appl. Phys. A **63**, 109 (1996)
8. M. Lenzner, J. Kruger, W. Kautek, F. Krausz, Appl. Phys. A **68**, 369 (1999)
9. K. Fuchs, Proc. Camb. Philos. Soc. **34** (1938)
10. E.H. Sondheimer, Adv. Phys. **1** (1952)
11. Q. Huang, W. Shen, W. Song, Synthesis of colourless silver precursor ink for printing conductive patterns on silicon nitride substrates. Appl. Surf. Sci. **258**(19), 7384–7388 (2012)
12. M.J. Webber, *Handbook of Optical Materials* (CRC Press, Boca Raton, 2003)
13. B. Mangote, L. Gallais, M. Zerrad, F. Lemarchand, L.H. Gao, M. Commandré, M. Lequime, Rev. Sci. Instrum. **83**, 013109 (2012)
14. J. Bonse, J.M. Wrobel, J. Kruger, W. Kautek, Appl. Phys. A **72**, 89 (2001)
15. Y. Jee, M.F. Becker, R.M. Walser, J. Opt. Soc. Am. B **5**, 648 (1988)
16. J. Byskov-Nielsen, J.M. Savolainen, M. Snogdahl, P. Balling, Appl. Phys. A **101**, 97 (2010)
17. Y. Dai, M. He, H. Bian, B. Lu, X. Yan, G. Ma, Appl. Phys. A **106**, 567 (2012)
18. M. Kimmel, P. Rambo, R. Broyles, M. Geissel, J. Schwarz, J. Bellum, B. Atherton, Proc. SPIE **7504**, 75041G (2009)
19. B. Rethfeld, K. Sokolowski-Tinten, D. Von Der Linde, S.I. Anisimov, Appl. Phys. A **79**, 767 (2004)
20. Y. Ren, J.K. Chen, Y. Zhang, J. Huang, Appl. Phys. Lett. **98**, 191105 (2009)
21. S.I. Anisimov, B.S. Luk'yanchuk, Phys. Usp. **45**, 293 (2002)
22. Z. Lin, L.V. Zhigilei, V. Celli, Phys. Rev. B **77**, 075133 (2008)
23. X.Y. Wang, D.M. Riffe, Y.-S. Lee, M.C. Downer, Phys. Rev. B **50**, 8016 (1994)
24. E. Leveugle, D.S. Ivanov, L.V. Zhigilei, Appl. Phys. A **79**, 1643 (2004)
25. D.S. Ivanov, B. Rethfeld, G.M. O'Connor, T.J. Glynn, A.N. Volkov, L.V. Zhigilei, Appl. Phys. A **92**, 791 (2008)
26. D.E. Hare, J. Franken, D.D. Dlott, J. Appl. Phys. **77**, 5950 (1995)
27. T.V. Kononenko, S.M. Pimenov, V.V. Kononenko, E.V. Zavedeev, V.I. Konov, G. Dumitru, V. Romano, Appl. Phys. A **79**, 543 (2004)
28. S.E. Kirkwood, A.C. Van Popta, Y.Y. Tsui, R. Fedosejevs, Appl. Phys. A **81**, 129 (2005)
29. P.T. Mannion, J. Magee, E. Coyne, G.M. O'Connor, T.J. Glynn, Appl. Surf. Sci. **233**, 275 (2004)
30. C.S. Lee, N. Koumvakalis, M. Bass, Appl. Phys. Lett. **41**, 625 (1982)